Environmental Modelling & Software 25 (2010) 770–781

Contents lists available at ScienceDirect

Environmental Modelling & Software

journal homepage: www.elsevier.com/locate/envsoft

TopoToolbox: A set of Matlab functions for topographic analysis

Wolfgang Schwanghart*, Nikolaus J. Kuhn

Physical Geography and Environmental Change, University of Basel, Klingelbergstrasse 27, 4056 Basel, Switzerland

ARTICLE INFO

Article history:
Received 7 May 2009
Received in revised form
23 November 2009
Accepted 6 December 2009
Available online 19 January 2010

Keywords:
Relief analysis
Flow networks
Digital elevation models
Linear algebra
Matlab
Graph Theory
Sparse matrices

ABSTRACT

TopoToolbox contains a set of Matlab functions that provide utilities for relief analysis in a non-Geographical Information System (GIS) environment. The tools have been developed to support the work flow in combined spatial and non-spatial numerical analysis. They offer flexible and user-friendly software for hydrological and geomorphological research that involves digital elevation model analysis and focuses on material fluxes and spatial variability of water, sediment, chemicals and nutrients. The objective of this paper is to give an introduction to the linear algebraic concept behind the software that employs sparse matrix computations for digital elevation model analysis. Moreover, we outline the functionality of the toolbox. The source codes are freely available in Matlab language on the authors' webpage (physiogeo.unibas.ch/topotoolbox).

Software availability

Program title: TopoToolbox
Developer: Wolfgang Schwanghart
First available: 2009
Source language: MATLAB
Requirements: MATLAB R2009a, Image Processing Toolbox
Availability: TopoToolbox is available free of charge and can be downloaded on http://physiogeo.unibas.ch/topotoolbox.

1. Introduction

The shape of the Earth's surface is of major concern to environmental scientists, and to geomorphologists and hydrologists, in particular. Relief is a product of endogenic and exogenic processes and human action that in combination create a variety of landforms. Landforms provide an access to the erosional and depositional past of the environment. As such, relief is an important archive of Earth's history. Relief, in addition, is the template for fluxes of water, sediment, chemicals and nutrients (Merritt et al., 2003; Callow and Smettem, 2009; Murray et al., 2009), and understanding the interactions between material fluxes and relief is a key to present environmental systems and their future evolution (Kuhn et al., 2009).

Digital elevation models (DEMs) form the basis of quantitative methods to analyze and model topography and its relation to geological, hydrological, biological and anthropogenic components of the landscape (Moore et al., 1993; Florinsky et al., 2002). As such, the analysis of DEMs is an essential method applied in morphometric analysis (Dikau, 1989; Klingseisen et al., 2008; Ames et al., 2009), prediction of soil properties (Florinsky et al., 2002) and ecological habitat characteristics (Beck and Kitching, 2009), distributed hydrologic modelling (Lacroix et al., 2002; Wu et al., 2007; Viviroli et al., 2009) and erosion and sediment transport modelling (Merritt et al., 2003).

A DEM usually is a finite set of georeferenced, irregularly or regularly spaced elevation points representing ground surface topography. Terrain is modelled with triangular irregular networks, contour vertices or hexagon tessellation. Most common, however, terrain is digitally represented as grids of squares because the regular data structure allows for simpler measurement algorithms (de By, 2001). Such algorithms are usually implemented in a Geographical Information System (GIS) software.

While GIS software provides powerful tools for spatial analysis, non-spatial analysis tools are usually deficient in GIS environments. Often, however, spatial and non-spatial analyses are combined when e.g. contaminant surveys, discharge measurements or soil carbon inventories meet relief analysis. In these cases flexible solutions are required to avoid large efforts in data exchange

* Corresponding author.
E-mail address: w.schwanghart@unibas.ch (W. Schwanghart).
URL: http://www.physiogeo.unibas.ch/

1364-8152/$ – see front matter © 2009 Elsevier Ltd. All rights reserved.
doi:10.1016/j.envsoft.2009.12.002

between different software packages. The solution presented here is TopoToolbox, a set of functions for topographic analysis implemented in Matlab programming language. TopoToolbox was designed to address the needs of researchers who analyze gridded DEM data to investigate material fluxes on Earth's surface. Matlab was chosen since it provides a versatile environment for mathematical and technical computing. It is based on a high-level programming language and as such, the functions provided here are easy to modify and open for amendments.

The major aim of this paper is to give an introduction to the linear algebraic concept for topographic analysis as implemented in TopoToolbox. The concept is explained using a miniature sample digital elevation model and various toolbox functions are illustrated. Finally, we present the functionality with a case study investigating stream discharge in the Upper Rhône Valley, Switzerland.

2. Digital elevation models, topographic attributes and their algebraic representation

2.1. Digital elevation models

DEMs are geographic field type of data that model topography and topographic change (Brooks, 2003). Most commonly DEMs are represented as rectangular grids where an elevation value is assigned to each cell. Mathematically this kind of data model is termed matrix. Matrices are rectangular tables of scalars termed elements. The elements of a matrix are referenced either by specifying rows and columns of each respective scalar in the matrix or by a linear, rowwise increasing index. Here, we adopt the latter referencing scheme. Consequently, elements in a DEM matrix **Z** are subscribed using linear indexing as shown in Fig. 1.

The geographic location of each DEM cell is determined by a coordinate system which assigns a projected location in the *xy*-plane to each element in the DEM matrix. Thus, the 2D-Euclidean distance *d* between two cells with the linear index *i* and *j* is calculated by

$$d_{ij} = \sqrt{(\mathbf{X}_i - \mathbf{X}_j)^2 + (\mathbf{Y}_i - \mathbf{Y}_j)^2} \quad (1)$$

with **X** and **Y** being matrices with the same size as **Z** where each element refers to the *x*- and *y*-coordinate, respectively.

Processes represented in hydrological and geomorphological cellular models are governed by local values like roughness coefficients, grain size or vegetation density contained in further matrices. When taking elevations into account, however, altitude in each cell is usually less important for process representations than the relation of a cell to each of its eight neighboring cells (Moore neighborhood). This relation is what we refer to as relief and which determines the type and intensity of lateral material fluxes such as gravitational processes.

Mathematically, neighborhoods can be represented in so called *adjacency matrices*. In *Graph Theory* these matrices are used to define edges between nodes of graphs (Bondy and Murty, 1976). An adjacency matrix $\mathbf{A(Z)} = [a_{ij}]$ of a DEM matrix **Z** with *n* elements is a symmetric $n \times n$ matrix, where the elements a_{ij} equal one when a cell with the linear index *i* is a neighbor of cell *j*. Otherwise, a_{ij} is zero. **A** is populated primarily with zeros ($>n^2-8n$) and can thus be classified as sparse. The sparse data structure allows for efficient storage organization and operations compute sparse results in time proportional to the number of arithmetic operations on nonzeros. Fig. 2a visualizes the sparsity pattern of **A** for the DEM **Z** displayed in Fig. 1.

Adjacency matrices and some modifications of them have a great value for DEM analysis. Some examples are explained in greater detail in the following sections.

2.2. Gradient

One of the most important factors of surface processes is gradient since it provides a measure for the potential energy in a specific location towards a local basis. The gradient of a DEM cell may be differently defined (Warren et al., 2004) but in many cases the trigonometrical maximum downward gradient is taken. Finding the maximum gradient requires the calculation of all slopes between all neighboring cells. The slope S_{ij} between two neighbor cells *i* and *j* is calculated by

$$S_{ij} = \frac{Z_i - Z_j}{d_{ij}} \quad (2)$$

where d_{ij} is the distance between the cells *i* and *j* as calculated in equation (1). Applied to all cells and their respective neighbor cells the results are transferred to a matrix **S** with *i* as row indices and *j* as column indices of the slope values. The resulting matrix **S** has the same sparsity pattern as the adjacency matrix **A**. This time, however, the nonzero elements contain the tangent of the slope that are – according to equation (2) – positive when indicating

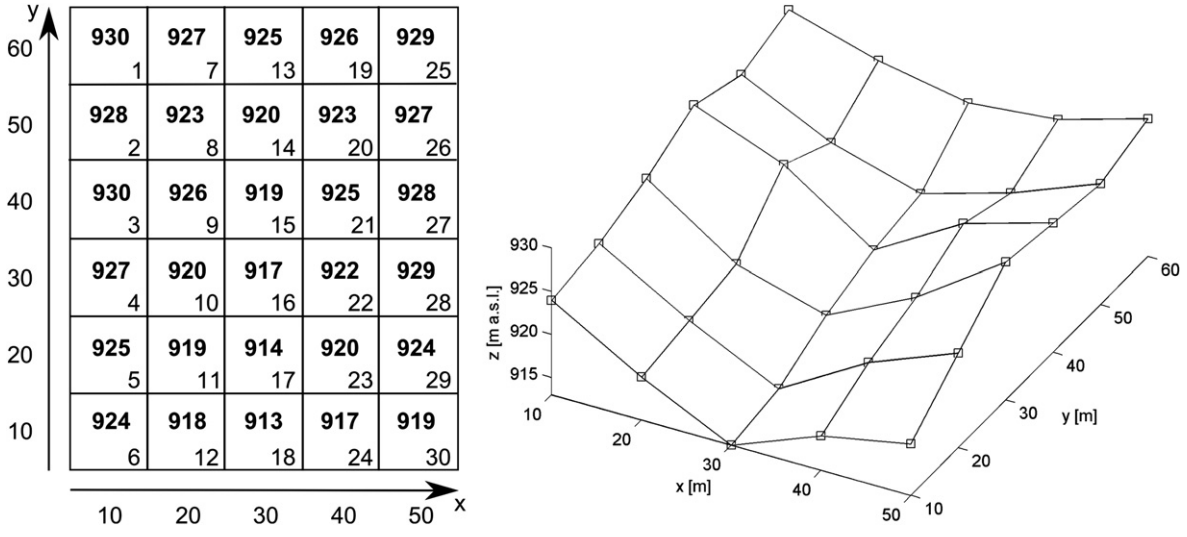

Fig. 1. Sample digital elevation model in matrix notation and surface illustration. Centered values in the matrix refer to cell elevation and lower right values refer to a linear index of the cells.

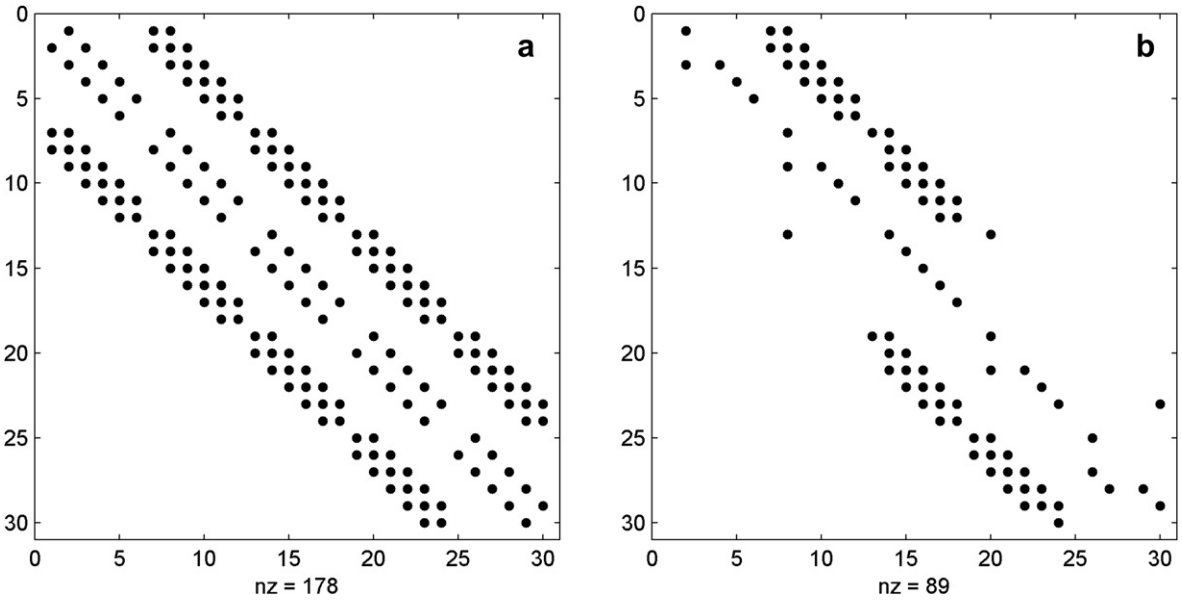

Fig. 2. Sparsity patterns of a) adjacency and slope matrix and b) multiple flow direction matrix of the sample DEM. Black dots refer to nonzero entries in the matrices.

a downward inclination between two neighbor cells. Hence, the sparsity pattern will be the same as the one of **A** (Fig. 2a) but the lower triangle values will be – 1 times the upper triangle values and vice versa. So, in contrary to **A**, **S** does not only indicate neighboring cells but also the type and magnitude of inclination between the DEM cells. Mathematically, the directional character of the slope matrix is expressed in $\mathbf{S} = (-1)\mathbf{S}^{\mathbf{T}}$. Finding the maximum downward gradient is easy now because only the maximum values along the second dimension of **S** must be found.

2.3. Flow direction

Flow direction determines the surficial movement of water, sediment and contaminants through terrain. Various algorithms have been proposed to determine flow directions (Tarboton, 1997; Orlandini et al., 2003; Seibert and McGlynn, 2007). The single flow direction algorithm (SFD, D8) states that water flows along the steepest gradient. SFD, however, often produces unrealistic, over-concentrated flow in topographic lows while divergent or braided flows are not represented (Nicholas, 2005). To overcome the weaknesses of SFD, a multiple flow direction algorithm (MFD) was developed. The MFD algorithm partitions and transfers discharge in each cell in multiple directions to all downward neighbor cells and thus allows for bifurcation and convergence of flow (Quinn et al., 1993; Arge et al., 2001; Coulthard et al., 2002).

Both single and multiple flow directions can be represented within the transfer matrix (**M**). Elements in **M** contain the relative amount of discharge M_{ij} transferred from one cell i to a maximum number of eight downward neighbors with the index j. Thereby the transfer ratios are proportional to the downward slope to the respective neighbor.

$$M_{ij} \sim \max\{S_{ij}, 0\} \tag{3}$$

M is created from the slope matrix **S** by replacing negative entries in **S** with zero. The removal of negative entries leads to a reduced sparsity pattern as displayed in Fig. 2b. Then nonzero entries are scaled along each row so that the sum in each row containing nonzero elements equals one. Row normalization of the transfer matrix is required to ensure conservation of mass when water exchange between cells is modelled.

In summary, **M** has following characteristics: (1) **M** is square. (2) **M** is sparse and all elements on the main diagonal are zero. (3) All elements in **M** are non-negative. (4) **M** is not symmetric. (5) The sum of all values in each row (along the second dimension) equals one or zero. The sum of ratios equals one when there is at least one downward located cell. If a cell is surrounded by higher neighbors only, it is a local minimum (sink) and the sum along the respective row in **M** is zero. The sum along columns of **M** depends on the location of the respective cell relative to its neighbors. Here, the sum refers to the sum of ratios each cell gains from its surrounding cells. A local maximum (summit) in a DEM will have zero contributing cells (e.g. cell 1 or 3 in the example). Cells with convergent flow will have sum values greater one.

The transfer matrix **M** exhibits many properties of transition probability matrices used in Markov chains (Davis, 1986). Yet, **M** contains rows summing to zero and its diagonal is occupied by zeros only. In a probabilistic sense, zeros on the main diagonal can be regarded as the zero probability that a cell retains fractions of its available water. **M** can also be described in graph theoretic terms. Since all directions point downward, **M** is an adjacency matrix of a weighted, directed, acyclic graph. As such, **M** is nilpotent, its eigenvalue equals zero and thus, it is not invertible. Yet, $\mathbf{I} - \mathbf{M}$, where **I** is the identity matrix, is always invertible and it is shown in the next section how this equation can be used to compute flow accumulation.

2.4. Drainage area

Drainage area is an important derivate of DEMs and its calculation is based on the information of flow direction. In order to derive drainage area, algorithms are required that determine how the topological, local flow rules act on larger distances. In GIS applications these algorithms are usually termed flow accumulation (FA) or upslope area algorithms. By counting the number of cells draining in each grid cell, FA algorithms calculate the upslope contributing drainage area which serves as measure for discharge in many modelling approaches. The estimation of the upslope contributing

area is dependent on the estimation of flow paths from a given cell as calculated from flow direction (Gallant and Wilson, 2000).

We show two ways to derive the upslope area from the flow direction matrix **M** using a set of coupled equations. First, we derive the linear system from the equilibrium equations of network flow without capacity constraints with the flow rates as unknowns. Second, we show that upslope area can also be represented as a geometrical, infinite progression of the flow direction matrix.

At constant inflow rates of 1 unit per unit time and area and steady state the flow at a point in the DEM equals the contributing upslope area at that point. Let w_i denote the storage of water in cell $i = 1, \ldots, n$ and f_{ij} the flow from cell i to j. Assume that each flow f_{ij} depends on storage w_i and distribution ratio m_{ij}. Then we gain the differential equation for the storage in each cell.

$$\frac{\mathrm{d}x_i}{\mathrm{d}t} = \sum_{j=0}^{n} f_{ij} - \sum_{j=0}^{n} f_{ji} = \sum_{j=0}^{n} m_{ij} w_i - \sum_{j=0}^{n} m_{ji} w_j \tag{4}$$

where $m_{ii} = 0$. f_{0i} and f_{i0} are exogenous inflow and outflow rates in each cell, respectively. At steady state the total inflow in each cell equals the outflow in each cell ($\mathrm{d}x_i/\mathrm{d}t = 0$) such that

$$\sum_{j=0}^{n} m_{ij} w_i - \sum_{j=0}^{n} m_{ji} w_j = 0. \tag{5}$$

The sum of the outflow ratios equals one ($\sum_{j=0}^{n} m_{ij} = 1$) in each cell i when there are any $m_{ij} \neq 0$. Otherwise, $m_{ij} = m_{0j} = 1$ and i is a sink. Incorporating this rule and calculating the steady state flow for a constant external inflow rate of f_{0i} in each cell i, equation (5) can be rearranged to

$$\sum_{j=1}^{n} w_i - \sum_{j=0}^{n} m_{ji} w_j = f_{0i}. \tag{6}$$

In matrix notation the equation becomes

$$\left(\mathbf{I} - \mathbf{M}^{\mathrm{T}}\right)\mathbf{w} = \mathbf{f0} \tag{7}$$

where **I** is the identity matrix and $\mathbf{M}^{\mathrm{T}}$ is the transpose of the flow direction matrix outlined above. **w** is a $n \times 1$ vector containing the storage values in each cell and **f0** is a $n \times 1$ vector where the values correspond to the inflow rates in each cell. Finally, solving for the storage in each cell rearranges equation (7) to

$$\mathbf{w} = \left(\mathbf{I} - \mathbf{M}^{T}\right)^{-1}\mathbf{f0} \tag{8}$$

The same equation can be derived from an infinite progression of a geometric series of $\mathbf{M}^{T}$. $\mathbf{w}(\mathbf{k})$ is a $n \times 1$ vector containing the storage of water at time step k. $\mathbf{w}(\mathbf{k})$ is a linear combination of $\mathbf{M}^{\mathrm{T}}$ and the water storage in the previous time step under the assumption that the velocity is constant throughout the spatial domain and all cells are equally distant.

$$\mathbf{w}(\mathbf{k}) = \mathbf{M}^{T}\mathbf{w}(k-1) \tag{9}$$

Iterating equation (9), the initial amounts of water in each cell are stepwise routed through the spatial domain as depicted in Fig. 3. After t time steps the water will have completely left the system and the amount in each cell $\mathbf{w}(\mathbf{t})$ is zero. A time series $w(0, 1, 2, \ldots, t)_i$ of a single cell i may consequently be regarded as a hydrograph at the respective location. The contributing drainage

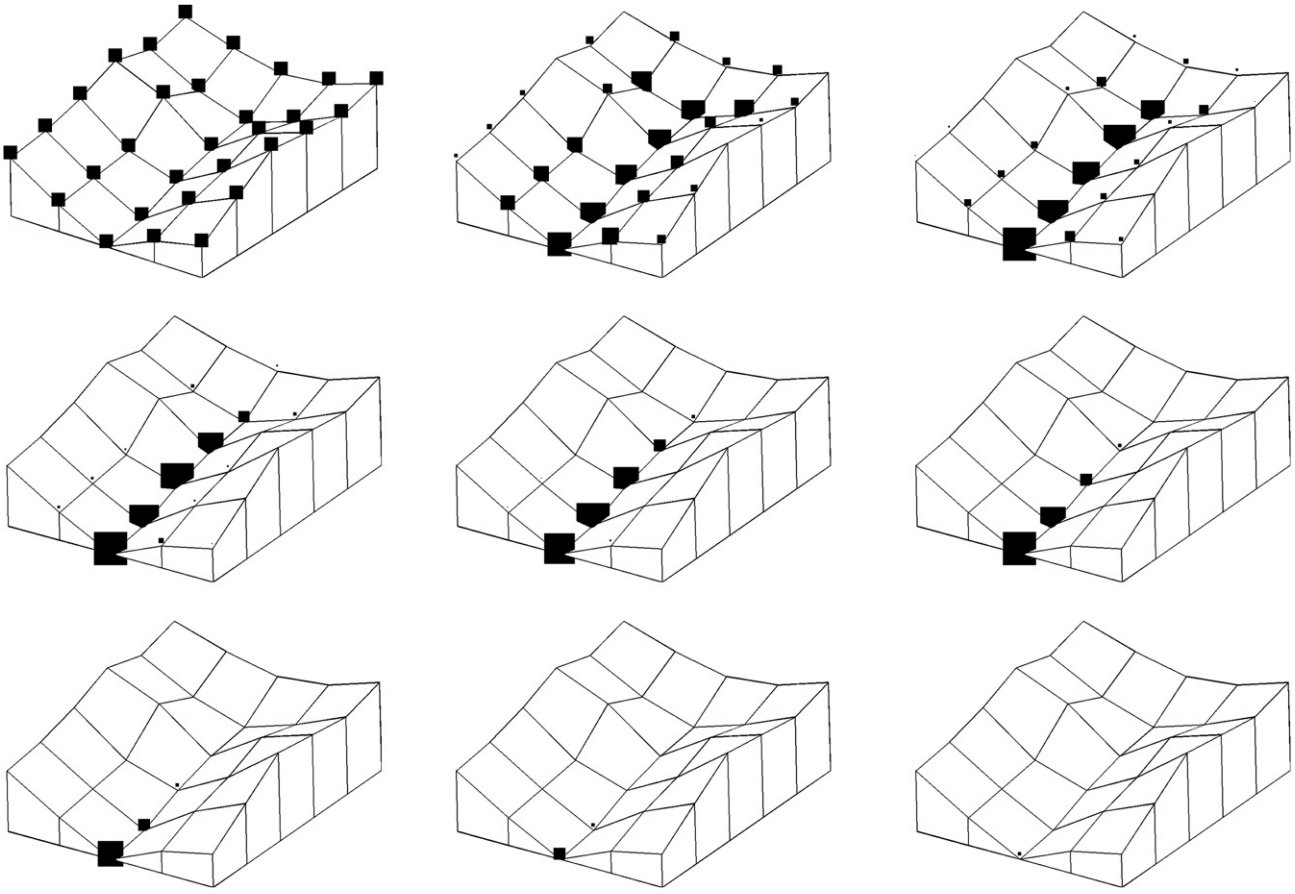

Fig. 3. Water routing through the sample DEM. Size of black squares indicate water amount proportional to the initial stage of 1 unit water in each cell (upper left).

area **a** of each cell is equivalent to the area under the cell's hydrograph and is calculated by adding the amounts in each cell during all time steps.

$$\mathbf{a} = \mathbf{w}(\mathbf{0}) + \mathbf{w}(\mathbf{1}) + \mathbf{w}(\mathbf{2}) + \ldots + \mathbf{w}(\mathbf{n}) \tag{10}$$

$$\mathbf{a} = \mathbf{w}(\mathbf{0}) + \mathbf{M}^{\mathrm{T}}\mathbf{w}(\mathbf{0}) + \mathbf{M}^{\mathrm{T}}\left(\mathbf{M}^{\mathrm{T}}\mathbf{w}(\mathbf{0})\right) + \ldots \tag{11}$$

$$\mathbf{a} = \left[\mathbf{I} + \mathbf{M}^{\mathrm{T}} + \left(\mathbf{M}^{\mathrm{T}}\right)^{2} + \ldots + \left(\mathbf{M}^{\mathrm{T}}\right)^{n}\right]\mathbf{w}(\mathbf{0}) \tag{12}$$

According to Strang (2003) such a geometric progression of a matrix is expressed as

$$\left[\mathbf{I} - \mathbf{M}^{\mathrm{T}}\right]^{-1} = \mathbf{I} + \mathbf{M}^{\mathrm{T}} + \left(\mathbf{M}^{\mathrm{T}}\right)^{2} + \ldots \tag{13}$$

The contributing upslope area vector **a** is consequently derived from the following equation system:

$$\mathbf{a} = \left[\mathbf{I} - \mathbf{M}^{\mathrm{T}}\right]^{-1}\mathbf{w}(\mathbf{0}) \tag{14}$$

$\mathbf{w}(\mathbf{0})$ is the initial amount of water in each cell and can be defined as $\Delta t\mathbf{f0}$. Upslope area can thus be mathematically defined in two ways. First, it can be determined as the steady state flow rate in each cell during a constant inflow to each cell of 1 unit per time unit. Second, it can be calculated from the integral of the hydrograph as a response to a unit amount of water rainfall event.

Two major advantages arise by using equation (8) or (14) when working with Matlab or other matrix computation software (Octave, Scilab, etc.). First, the linear system of equations can be efficiently computed by matrix left division algorithms (the back slash operator in Matlab). Matlab determines $\mathbf{I} - \mathbf{M}^{\mathrm{T}}$ to be a permutation of a triangular matrix and solves the system using a permuted backsubstitution algorithm. Second, the user can easily define spatially variable initial water amounts by modifying $\mathbf{w}(\mathbf{0})$.

3. The TopoToolbox

3.1. Overview

TopoToolbox contains various functions for DEM, flow pattern analysis and sub-basin analysis (Table 1). Besides import and export functions that support the ESRI ascii grid standard, TopoToolbox provides functions for DEM manipulation, such as a sink fill algorithm and functions for the derivation of topographic derivates (e.g. hillshading, slope and curvature). A set of functions serves the calculation of the flow direction matrix (see next section), which serves as the central input argument for various other functions.

3.2. Calculation of the transfer matrix

The graph theoretic concept outlined in the section above is the basis for many of the functions listed in Table 1. Hence, the transfer matrix **M** is of eminent importance for further calculations. The derivation of **M**, however, is not as straightforward as outlined above. Assigning flow directions to cells is possible as long as they have downslope cell neighbors. This is not always the case and topographic depressions and pits caused by DEM irregularities result in flow discontinuities. Algorithms have been proposed to route flow through pits (Temme et al., 2006) and to break flow obstructions by outlet breaching (Kenny et al., 2008), but usually pits are filled using flood fill algorithms and the flow routing procedures involve algorithms that generate flow paths across flat terrain.

The toolbox features two algorithms for routing over flat terrain (Fig. 4). Routeflats is a recursive, upstream flow path generator that returns both single and multiple flow directions on flat terrain, and impedes cycles in **M**. While this algorithm returns continuous flow patterns, it is computationally demanding especially when the DEM features large connected components of flat terrain such as lakes. Crossflats overcomes these problems by directly connecting cells at the interface between flat terrain and adjacent upward slopes and cells at the outlet of the flat terrain (Fig. 4). While crossflats preserve connectivity of flow pathways, it excludes cells in flat terrain for the benefit of computational costs. The application of crossflats is especially expedient when large areas of flat terrain dominate the DEM.

TopoToolbox allows the user to exert control on the flow matrix derivation. The control involves the user's choice between MFD and SFD algorithms, edge handling, flow direction randomization and concentration. By default, flow direction at the grid boundaries is inwards to lower neighbor cells and local minima on the grid

Table 1
Functions in TopoToolbox.

Function name	Description
I/O functions	
Rasterread	Read/import ESRI ASCII grid
Rasterwrite	Write/export data to ESRI ASCII file
Digital elevation model correction/manipulation	
Crossflats	Crossflats of a digital elevation model
Demsmooth	Mean filter a digital elevation model with a kernel
Fillsinks	Fill/remove pits, sinks or topographic depressions
Routeflats	Route through flats of a digital elevation model
Topographic derivates	
Curvature	8-connected neighborhood curvature of a digital elevation model
Dependencemap	Drainage area for specific locations in a digital elevation model
Drainagebasins	Segment a digital elevation model in drain basins/catchments
drainagedensity	Calculate drainage density of individual drainage basins
Ezflowacc	Easy to use flow accumulation algorithm for Digital Elevation Models
flowacc	Calculate flow accumulation/upslope area from flow direction matrix
Flowacc_lm	Flow accumulation (upslope area) for LARGE Digital Elevation Models
Flowconvergence	Compute flow convergence of a digital elevation model
Flowdir	Multiple and single flow direction algorithm
Flowdir_single	Single flow direction algorithm
Flowdistance	Compute flow distance to cell or to catchment outlet
Flowdistanceds	compute downstream flow distance from a cell
Gradient8	8-connected neighborhood gradient and aspect of a digital elevation model
Hillshade	Create hillshading from a digital elevation model
Identifyflats	Identify flat terrain in a digital elevation model
Influencemap	Downslope area for specific locations in a digital elevation model
multi2single	Convert multiple to single flow direction matrix
Multiremfracs	Remove small fractions in a multiple flow direction matrix
Streamorder	Calculate Strahler Stream Order from flow direction matrix
Sub-basin analysis	
Sbplot	Plot sub-basins and connectivity between sub-basin gauges
Sbprops	Measure properties of sub-basins
Sbstruct	Create structure array for sub-basin analysis
Flow path analysis	
Flowpathbuffer	Create a buffer around a stream and extract indices of cells
Flowpathextract	Extract linear indices of a single Flow path in a DEM
Other tools	
Coord2ind	Convert xy coordinates to linear index
Ixneighbors	Neighbor indexing in a matrix
Usersguide	Introductory script to the toolbox

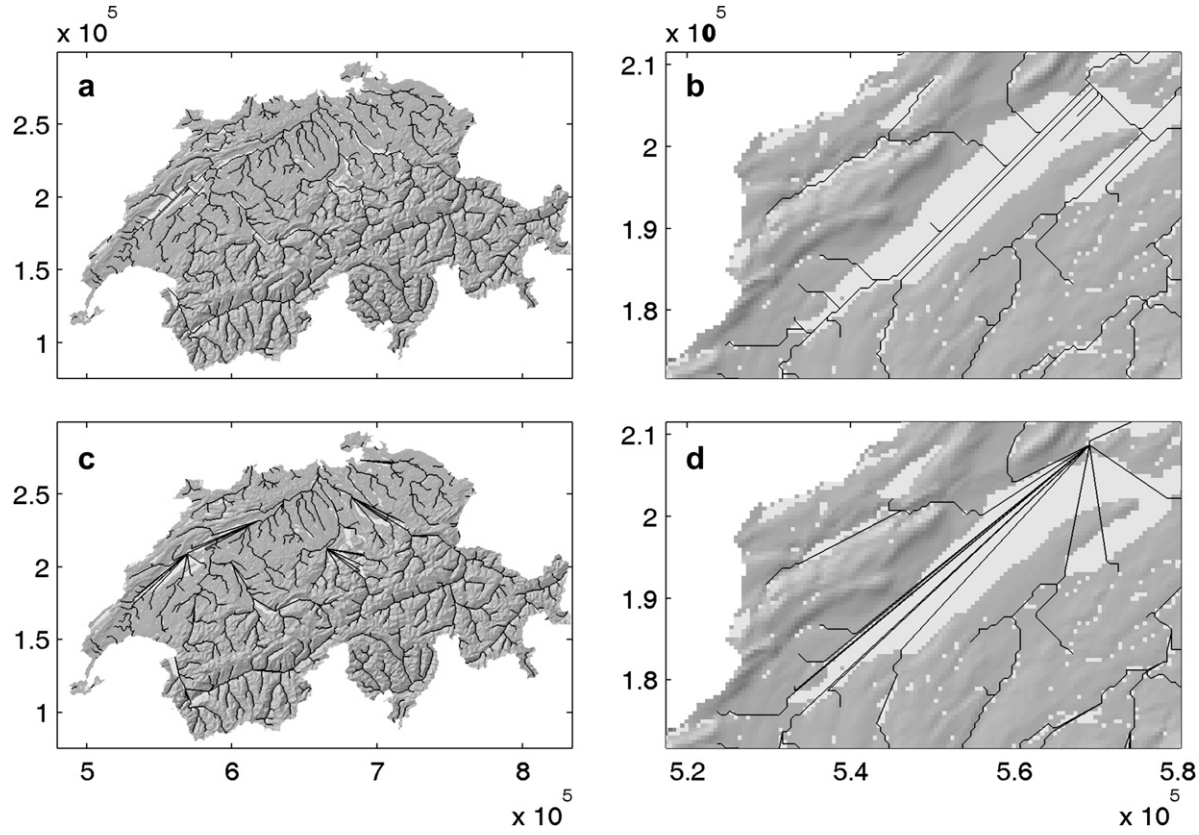

Fig. 4. Flat routing by two different algorithms in TopoToolbox. a) and c) Hillshade of the Swiss DEM. Bright, contiguous areas indicate flat areas such as lakes. Black lines represent the drainage network generated by routeflats and crossflats, respectively. b) and d) Detailed views of both routing mechanisms across the Neuenburger See (Lac Neuchâtel).

boundaries act as sinks. Closed boundaries may sometimes lead to overestimation along the grid edges. In this case open boundaries may be defined where the outflow of each cell (see equation (4)) is adjusted so that

$$-\sum_{j=0}^{n} f_{ji} = -\sum_{j=0}^{n} \frac{n_j}{8} m_{ji} w_j \tag{15}$$

where n_j is the number of neighbor cells of cell j.

Flow direction randomization means the addition of a stochastic component to the flow direction in order to impair the slope dependence of the drainage direction of each cell (Fairfield and Leymarie, 1991). Flow direction randomization provides a means to account for uncertainties in the DEM that affect drainage pathways in relief with low variability and for highly variable flow processes such as those prevailing in arid regions. Flow concentration facilitates the control of flow dispersion in the MFD algorithm by applying different weights to slopes. Exponentiation by a real valued factor larger one and subsequent row-standardization of **M** gives higher weights to steeper slopes and reduces dispersion in variable terrain.

3.3. Sub-basin analysis

A set of tools of TopoToolbox is dedicated to sub-basin analysis. Sub-basins refer to spatial units that comprise the surface contributing area of a specific site in the DEM. Sub-basins are often required to parameterize aggregated simulation areas in semi-distributed hydrological models (Lacroix et al., 2002; Merritt et al., 2003). While many software solutions are incapable of processing sub-basin outlets to specified locations, sub-basin analysis in TopoToolbox can consider numerous, user-defined outlet locations such as several stream flow gauges within one basin.

Sub-basin analysis is based on processing a structure array that contains each sub-basins' linear indices of cells that drain towards the proximate sub-basin outlet. In addition, the structure array contains information on the network topology arranged by the sub-basin outlets stored as adjacency matrix. The user can thus choose between two modes of sub-basin analysis: aggregated and non-aggregated analysis. While aggregated sub-basin analysis allows for the calculation of various statistical parameters within the total contributing area of a specific gauge, non-aggregated analysis restricts analysis to the proximate contributing pixels, that do not contribute to another upstream gauge. An example of non-aggregated sub-basin analysis combining spatial and non-spatial analysis is provided in the following case study.

4. Case study

4.1. Introduction

In this section we illustrate the performance of TopoToolbox with a combined application of spatial and non-spatial data analysis using a case study on the Upper Rhône basin in Switzerland (Fig. 5). The major aim of the analysis is to evaluate the suitability of the grid-based data set of mean monthly runoff depths made available by the Swiss Federal Office for the Environment (FOEN) and the Swiss Federal Institute for Forest, Snow and Landscape Research (WSL) (Pfaundler and Zappa, 2006) for stream discharge estimation. The gridded runoff data has been generated to facilitate discharge estimation in ungauged basins. Careful validation of the gridded discharge has been undertaken by Pfaundler and Zappa (2006)

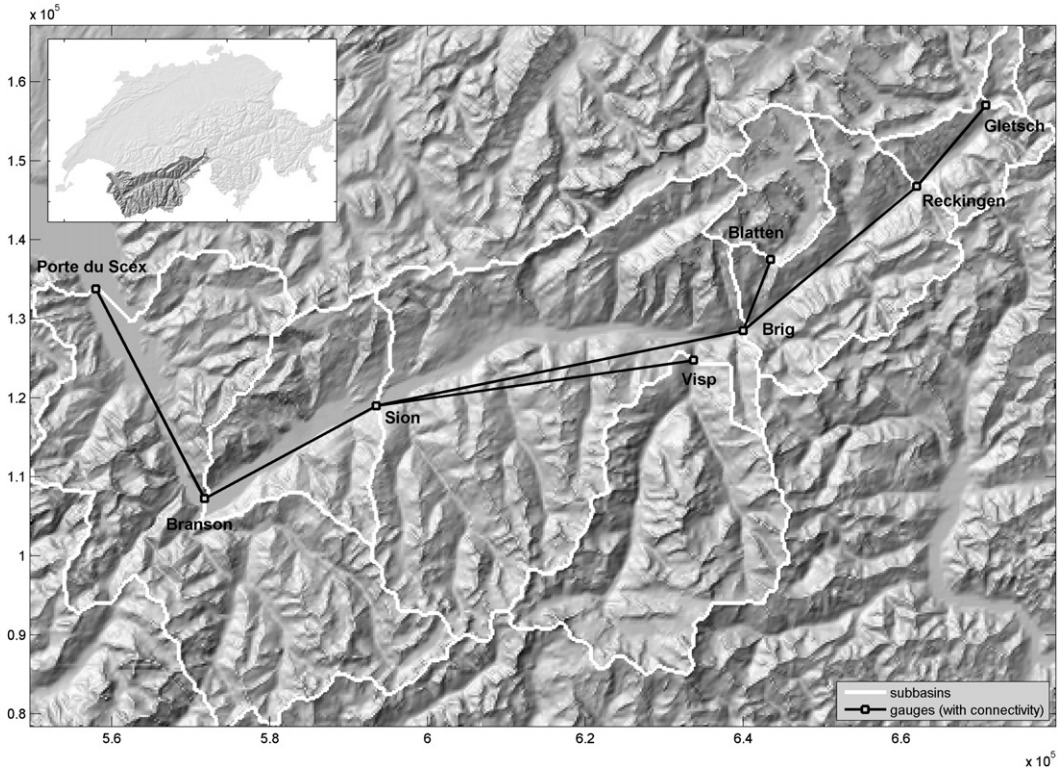

Fig. 5. Relief map of the Upper Rhône basin and topology of the stream gauge network. Sub-basins of gauges are demarcated by white lines. The coordinate system of the map is the Swiss Grid CH1903 (units: m).

for mesoscale basins (5–500 km^2), yet to our knowledge it has never been attempted to test the data set for large basins. Thus, our objectives are (1) the development of an approach to assess spatial sources of uncertainty using data derived from a network of stream gauges and (2) to identify the underlying causes behind error variance.

The study site comprises the Upper Rhône Valley (ca. 5300 km^2) above Lake Geneva. We chose this site since it is a non-karstic environment where topography is expected to determine flow direction to a great extent (Pfaundler and Zappa, 2006). Moreover, the basin hosts different runoff regimes (glacial, nival and pluvial).

4.2. Data and methods

We used a DEM with 250 m resolution covering the Upper Rhône basin (Fig. 5). Mean monthly runoff for the period 1981–2000 was obtained from the 500 m grid made available by the FOEN and WSL (Pfaundler and Zappa, 2006). The data set has been generated by the reconciliation of results from the spatially distributed hydrological model PREVAH (Precipitation–Runoff–Evapotranspiration HRU related Model) (Gurtz et al., 1997; Zappa et al., 2003; Verbunt et al., 2005; Viviroli et al., 2009) and a simulation experiment for the detection of evapotranspiration (Zappa, 2002). The data is available online (http://www.bafu.admin.ch/hydrologie/01832/01855 (3 November 2009)). The data was upscaled to fit the DEM extent and resolution using linear interpolation and units were set to m^3 s^{-1}.

Daily discharge data for eight stream gauges (Fig. 5) and metadata (glaciated area, basin area) in the Upper Rhône basin were obtained from FOEN and aggregated to monthly mean values for the period 1981–2000. Data on major water reservoirs were taken from the Hydrological Atlas of Switzerland (http://hades.unibe.ch/hades_d/ (3 November 2009), Spreafico et al. (1992)) and geocoded using Google Earth.

At a first step, we calculated flow direction and accumulation for the study site and compared flow patterns with stream features in a 1:200,000 topographic map. We found that stream directions were captured very well by the flow direction algorithm. The surface contributing area of each station was compared to the area indicated in the gauge metadata. The RMSE is 32.7 km^2 and the relative deviation ranges between −4.2 and +1%. Subsequently, sub-basins for each stream gauge and their topology (Fig. 5) were determined (sbstruct) and mean monthly discharge values were summed for each sub-basin using the non-aggregation mode of (sbprops). A correction factor CF_i for each sub-basin i was derived by comparing gauge discharge with aggregated sub-basin discharge by solving following equation system:

$$q_{\mathrm{meas},i} = \sum_{j=1}^{n} \mathrm{CF}_j \cdot \begin{cases} q_{\mathrm{agg},j} & \text{if } j \subseteq k_i \\ 0 & \text{otherwise} \end{cases} \tag{16}$$

where $q_{\mathrm{meas},\,i}$ is the measured discharge at gauge i, $q_{\mathrm{agg},\,j}$ is the aggregated runoff in each sub-basin j and k_i is the subset of gauges within the catchment of i. The correction factor denotes the value by which the aggregated discharge in each sub-basin must be multiplied to balance the gauge discharge. Hence, if CF_i equals one then there is a perfect match between estimated runoff and runoff contributed to stream discharge in sub-basin i. Values greater than one and less than one denote under- and overestimation, respectively. Correction factors were calculated for each month.

In order to assess causes for under- and overestimation, we aimed at modelling the correction factor for each sub-basin and month using partial least squares regression (PLS) (Wold, 1975) (plsregress). We chose PLS since it is typically recommended in situations in which the sample size is small compared to the

number of predictor variables (Haenlein and Kaplan, 2004). The PLS was calculated for four, standardized predictor variables available for each sub-basin (surface ratio affected by reservoirs, total capacity of reservoirs, glaciated surface ratio and mean elevation as surrogate for water retainment and release by snow) and two PLS components. Prior to PLS calculation the CF was logtransformed. Interpretation of the PLS results is based on the regression coefficients of the predictor variables on the CF.

The modelled CF_{est} was used to estimate gauge discharge $q_{est,\,cf}$ by solving following equation

$$q_{\mathrm{est,cf},i} = \sum_{j=1}^{n} \mathrm{CF}_{\mathrm{est},j} \cdot \begin{cases} q_{\mathrm{agg},j} & \text{if } j \subseteq k_i \\ 0 & \text{otherwise} \end{cases} \tag{17}$$

where the notation refers to equation (16).

4.3. Results and interpretation

In general, there is a good agreement between monthly mean gauge discharge and accumulated runoff for each gauge basin (Fig. 6). Yet, according to the curved annual course of the modelled values around the 1:1 line, the model systematically under- and overestimates stream discharge during the winter and summer months, respectively (Fig. 6). The spatial and temporal characteristics of this bias manifest themselves in the CF (Fig. 7). According to the CF the contribution of various sub-basins to stream discharge is underestimated by factors greater than eight during winter. An explanation for this behavior is partly provided by the operation of water reservoirs for power generation and flood control that can retain up to 25% of the annual discharge and lead to an increase of winter discharge and reduction of summer flows (Loizeau and Dominik, 2000; Fette et al., 2007). The different annual course of the CF for Blatten affirms this hypothesis since the Massa River is not impounded upstream to the gauge. Yet, a solely reservoir induced bias must be excluded since Gletsch features the aforementioned bias despite its reservoir-free basin.

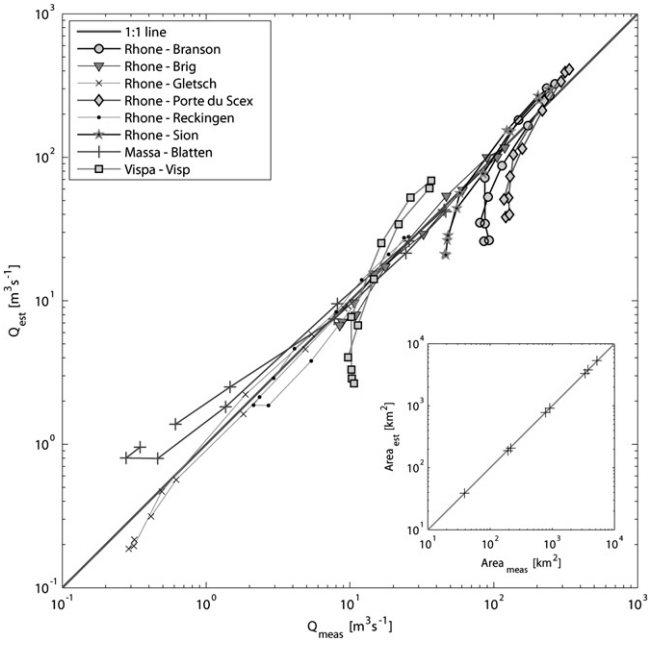

Fig. 6. Large plot: comparison of measured stream discharge and estimated discharge for each month and gauge. Lines indicate the annual course of discharge for different stations and point to the bias in the estimates during the summer and winter months. Small plot: comparison of measured and estimated basin area for each gauge.

In order to assess the origin of the bias four variables were included in the PLS to explain the temporal and spatial behavior of the CF. As shown in Fig. 8 a model with two latent factors explains a substantial part (RMSE ranges between 0.14 and 0.61) of the variance in CF. The PLS coefficients are depicted in Fig. 9. During the winter and early spring months the CF is positively related to the surface ratio affected by reservoirs in each sub-basin. This relation supports the notion of water release from reservoirs during this time. The total reservoir volume in each sub-basin provides only few explanatory power (Fig. 10).

The relation between reservoir affected areas is reversed from June to October. Intense reservoir filling by snow and glacier ice melting reduce stream discharge and sub-basins with large reservoir capacities and areas affected by water retention contribute less to stream flow.

Throughout the year, the CF is nearly exclusively negatively correlated to the glaciated surface ratio and mean elevation of sub-basins. We interpret this relation to reflect a general runoff overestimation from glaciated regions and elevations with high snow cover. This general overestimation over the annual course was also asserted by Pfaundler and Zappa (2006).

Recalculating stream discharge using the modelled CF (see equation (17)) shows a general improvement in the reproduction of the annual discharge course at the gauges. In particular gauges such as Porte du Scex, Branson and Sion that are affected by a combination of various factors benefit from more accurate discharge estimates.

4.4. Discussion and remarks

The results presented are based on an analysis with only few data. Hence, they may be limited in their universality and transferability. Our aim, however, was to present an example of a combined spatial and non-spatial analysis that enables us to explain temporal and spatial patterns observed in a runoff data set. The analysis demonstrates the effects exerted on stream discharge by the operation of reservoirs and provides an explanation for error variance in the gridded runoff data. Finally, the application of a modelled CF for each sub-basin improves the estimation of stream discharge.

Uncertainties in the final discharge estimates can be attributed to various factors. The predictive variables on reservoirs comprise only the largest reservoirs and we cannot exclude effects on stream discharge by smaller scale water retention, withdrawal for agriculture and redirection which are not covered by the data set. Groundwater dynamics, especially seasonal changes in floodplain storage (Fette et al., 2004), effect stream discharge, but variables describing these dynamics were not available for the analysis.

Despite these limitations, we show that stream discharge estimations can be improved by incorporating variables that explain the structural characteristics of sub-basins. Stream discharge estimations in ungauged basins based on the gridded runoff data set should therefore include corrections based on structural basin characteristics such as glaciated areas and reservoir affected areas to be reliable. We suggest to estimate correction factors for gauged basins and apply them to ungauged basins. This, however, requires more comprehensive discharge data than was available for this case study.

The analysis mainly relied on the analysis of the network structure of sub-basins that enabled the analysis of the components and their contribution to a drainage network. The implementation of the analysis within a computational environment for both spatial and non-spatial analysis using TopoToolbox was expedient since Matlab provides various non-spatial analysis techniques and data arrays such as structure and cell arrays that allow for data models

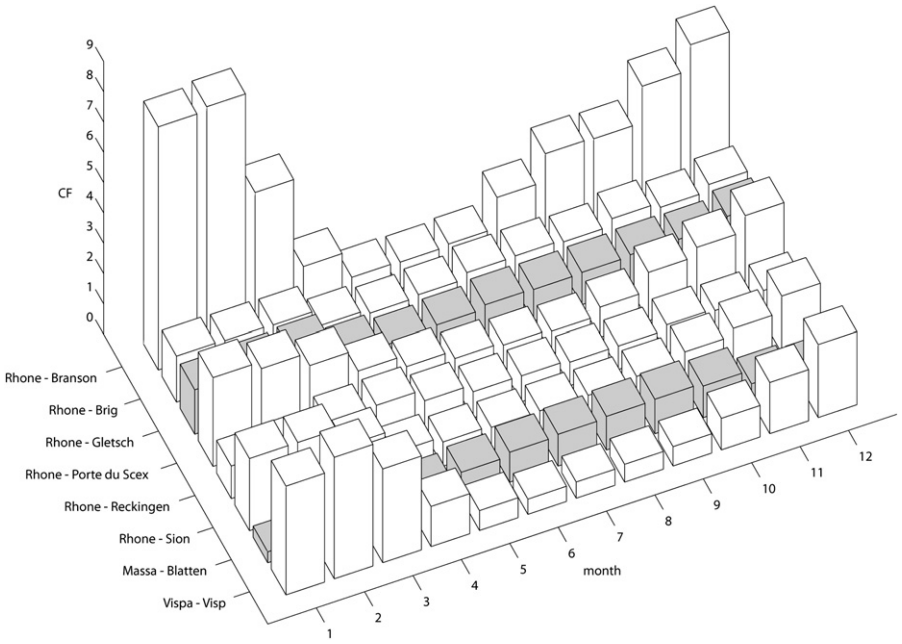

Fig. 7. Correction factors for stream discharge estimates for each gauge and month (see text for further explanation). Gray bars indicate gauges with basins not affected by reservoirs.

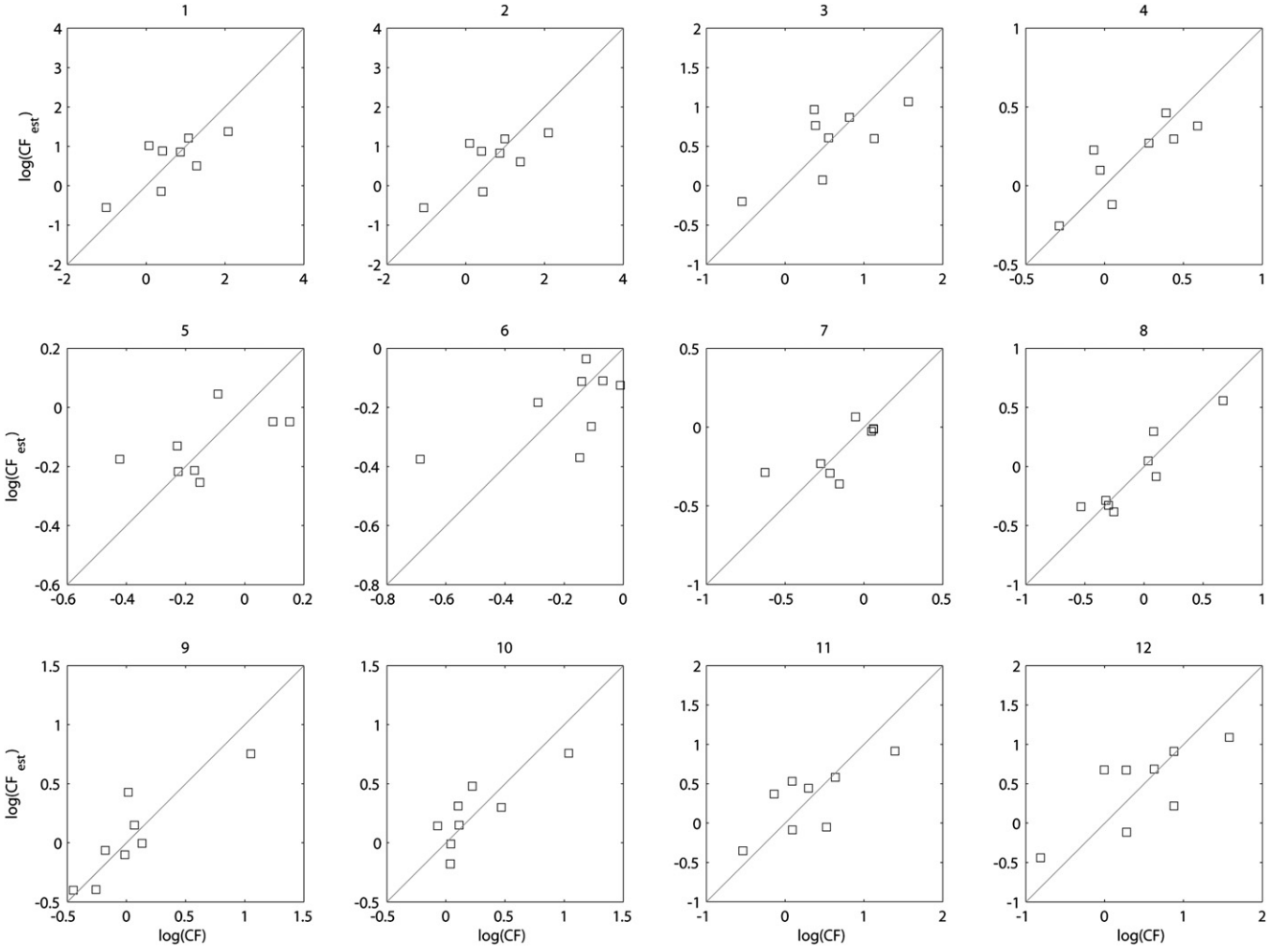

Fig. 8. Comparison of correction factors (CF) and estimated correction factors (CF_{est}) for each month.

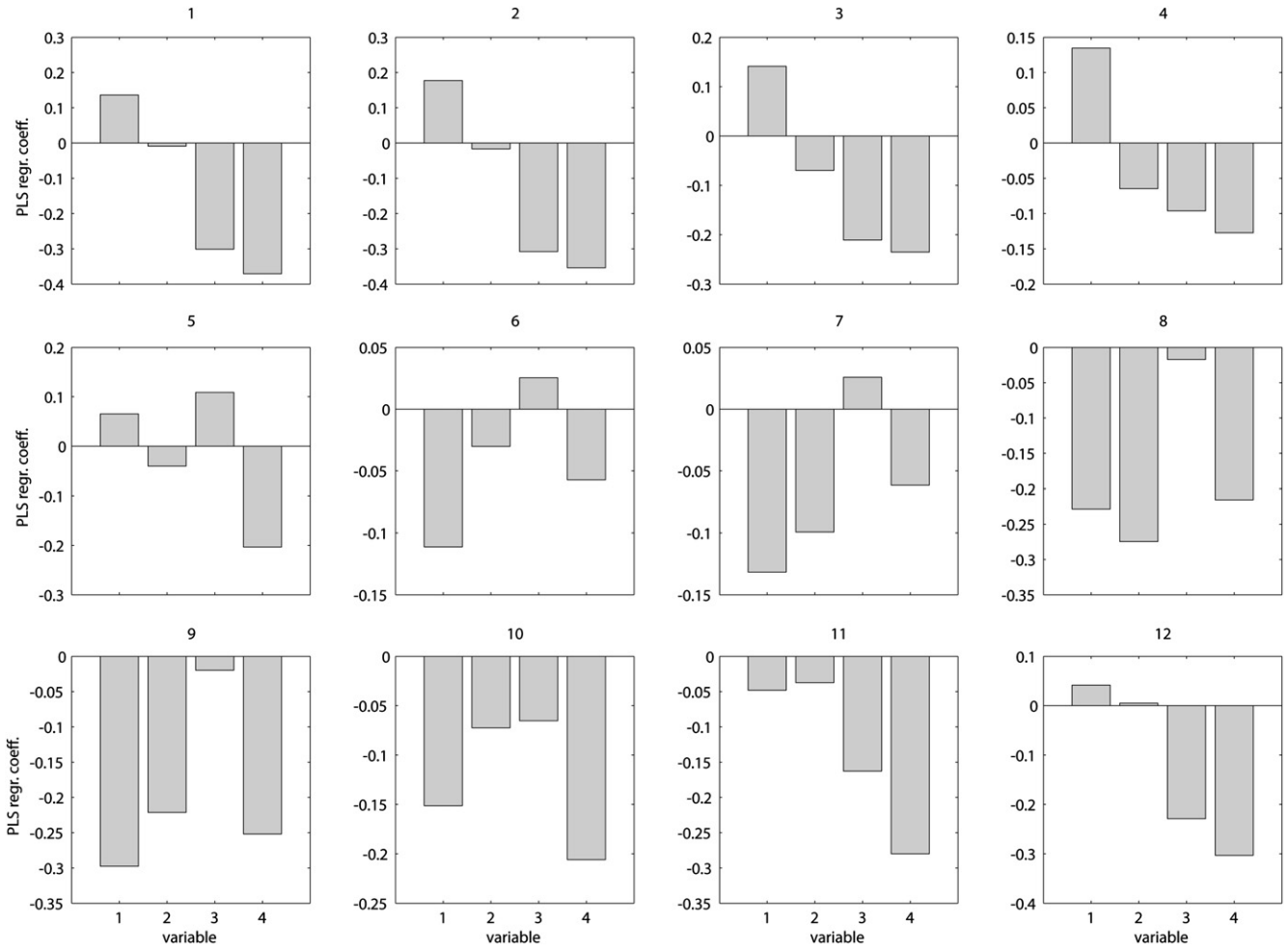

Fig. 9. Partial least squares regression (PLS) coefficients for each month. Variables included in the PLS were (1) surface ratio affected by reservoirs, (2) total capacity of reservoirs, (2) glaciated surface ratio and (3) mean elevation.

beyond conventional geospatial formats (raster and vector data) such as graph theoretical models.

5. Discussion

The integration of spatial and non-spatial analysis software aims at providing a combination of the most efficient and powerful tools available in both environments (Brenning, 2008). There are various examples where this has been accomplished using access links between different software packages. JGrass, for example, provides integration of the statistic R package into the scripting environment (Rigon et al., 2008). RSAGA provides access to SAGA GIS geoprocessing functions from within the R statistical data analysis environment (Brenning, 2008). So far, Matlab does not include any spatial modelling capability (Pullar, 2004). As such, TopoToolbox is a recent contribution to the endeavor for combining powerful GIS tools for geomorphical and hydrological application with the vast functionality of Matlab and, thus, addresses primarily users that have already gained experience in working with Matlab.

Integrating GIS analysis tools into the Matlab environment has various advantages, but suffers also from important limitations. Most importantly, virtual memory limitations set constraints to the size of DEMs that can be used with TopoToolbox. Matrix operations in Matlab are optimized for double precision data and sparse matrices only support logical and double precision data so far. Moreover, disk caching techniques such as applied by ArcGIS are difficult to implement. With respect to data size, TopoToolbox thus cannot compete with many systems that support one or two orders of magnitude larger DEMs. Out-of-memory issues usually arise when calculating the MFD matrix for large grids (more than 1000 rows and columns), since the sparse matrix requires approx. 6.5 times more memory than the DEM (the SFD matrix requires twice more memory than the DEM). Upslope area computation for large grids based on the MFD matrix, however, has been facilitated in TopoToolbox using a tiling approach (flowacc_lm). Another limitation is speed performance that becomes eminent for iterative algorithms used in the toolbox. The speed limitation will be particular evident in older Matlab Versions since the just-in-time (JIT) acceleration was first introduced in Matlab Version 6.5.

TopoToolbox requires Matlab and the Image Processing Toolbox (IPT). While various functions do not specifically need the IPT, fillsinks, for example, is based on fast image processing algorithms of morphological reconstruction (Vincent, 1993). While the IPT requirement limits the application of TopoToolbox to selected users, the deployment of the IPT functions ensures the use of fast and stable algorithms.

There are several advantages of the Matlab implementation of TopoToolbox. Matlab runs on different operating systems (Windows, Mac, Linux, Sun) and the mere implementation of the

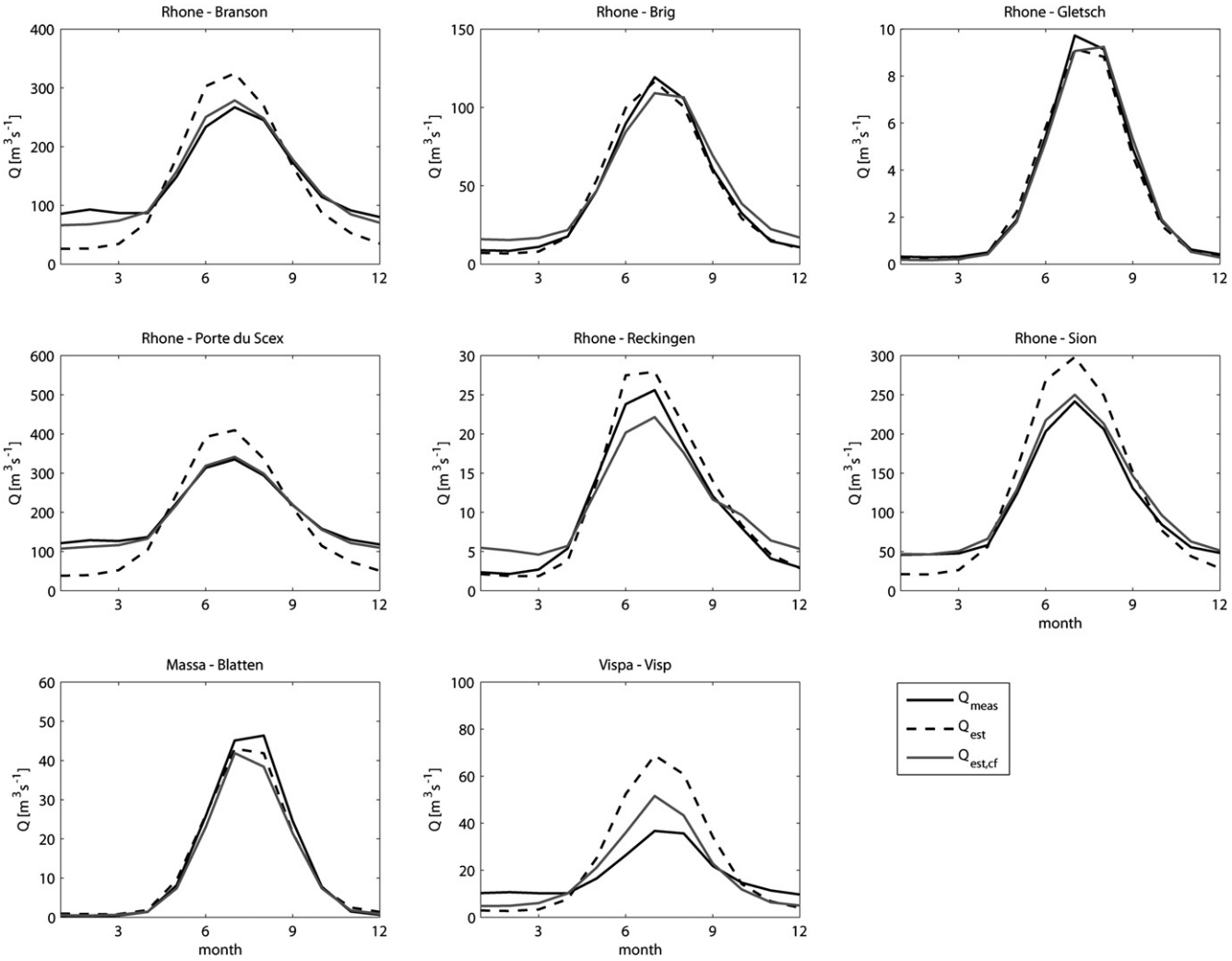

Fig. 10. Comparison between measured monthly stream discharge (Q_{meas}), stream discharge estimates based on gridded runoff data (Q_{est}) and stream discharge estimates based on gridded runoff data with modelled correction factor ($Q_{meas,\ cf}$).

function as Matlab code enables TopoToolbox to run on all of these platforms without the need for compilation. Matlab is a powerful tool for software development and the language is relatively easy to learn. It contains a large collection of functions from different scientific and technical fields such as image and signal processing and statistics that revert to state-of-the-art libraries for matrix and sparse matrix computation. By employing the functions added by TopoToolbox, DEM analysis is facilitated in a versatile environment and can be directly combined with non-spatial data analysis and various visualization tools. Moreover, TopoToolbox promotes software integration and customizing with comparatively low effort because both developer and users are not urged towards working with low-level programming languages.

So far, the flow direction algorithms implemented in TopoToolbox are the SFD and MFD algorithms. These algorithms tend to produce too linear and too dispersive flow patterns, respectively (Tarboton, 1997; Seibert and McGlynn, 2007). Flow randomization and concentration as implemented in TopoToolbox provide means to control this unrealistic behavior. Yet, other algorithms based on triangular facets have been developed to overcome these weaknesses (Tarboton, 1997; Seibert and McGlynn, 2007; Pelletier, 2008). These algorithms can be transferred to the linear algebraic approach outlined here and software that implements these algorithms have been made available on the Mathworks File Exchange (http://www.mathworks.com/matlabcentral/, #15818) by Steve Eddins together with various other functions.

TopoToolbox is under constant development and future versions will include more functionalities than outlined above. Moreover, we encourage users to provide feedback, requirements and ideas on existing and new developments.

6. Conclusions

TopoToolbox was designed to address many of the specific needs of researchers who analyze gridded DEM data. Here, we provide an overview on the linear algebraic concept of DEM analysis as implemented in the software and give an example of its usage. The main advantages of the software are to offer tools for topographic analysis in a versatile environment. As such, users have the opportunity to adapt the algorithms to their own needs and to combine spatial analysis with non-spatial analysis in a single environment. Owing to the simple structure of the software, adding new options, routines and functions is a straightforward task. Updating and extending the toolbox functions will be ongoing and users and developers are welcome to contribute ideas on improvements and new utilities.

Acknowledgments

We are particularly grateful for helpful and inspiring discussions with Steve Eddins from The Mathworks and many contributors to the file exchange who shared knowledge and ideas for the implementation of this toolbox. We are grateful to Riccardo Klinger from the Geographical Institute at the Freie University of Berlin for testing and commenting on this toolbox and for providing helpful discussions on the manuscript.

References

Ames, D.P., Rafn, E.B., Kirk, R.V., Crosby, B., 2009. Estimation of stream channel geometry in idaho using gis-derived watershed characteristics. Environmental Modelling & Software 24 (3), 444–448.

Arge, L., Chase, J., Halpin, P., Toma, L., Urban, D., Vitter, J., Wickremesinghe, R., 2001. Flowcomputation on massive grid terrains.

Beck, J., Kitching, I.J., 2009. Drivers of moth species richness on tropical altitudinal gradients: a cross-regional comparison. Global Ecology and Biogeography 18, 361–371.

Bondy, J.A., Murty, U.S.R., 1976. Graph Theory with Applications. Elsevier, New York, Amsterdam, Oxford.

Brenning, A., 2008. Statistical geocomputing combining r and saga: the example of landslide susceptibility analysis with generalized additive models. In: Böhner, J., Blaschke, T., Montanarella, L. (Eds.), SAGA – Seconds Out. Hamburger Beiträge zur Physischen Geographie und Landschaftsökologie, vol. 19. Hamburg University, Hamburg, pp. 23–32.

Brooks, S.M., 2003. Slopes and slope processes: research over the past decade. Progress in Physical Geography 27, 130–141.

de By, R.A. (Ed.), 2001. Principles of Geographic Information SystemsITC Educational Textbook Series, second ed., No. 1. ITC, Enschede, The Netherlands.

Callow, J., Smettem, K., 2009. The effect of farm dams and constructed banks on hydrologic connectivity and runoff estimation in agricultural landscapes. Environmental Modelling & Software 24 (8), 959–968.

Coulthard, T., Macklin, M., Kirkby, M., 2002. A cellular model of holocene upland river basin and alluvial fan evolution. Earth Surface Processes and Landforms 277, 269–288.

Davis, J.C., 1986. Statistics and Data Analysis in Geology, second ed. John Wiley & Sons, New York, Chichester, Brisbane.

Dikau, R., 1989. The application of a digital relief model to landform analysis in geomorphology. In: Raper, J. (Ed.), Three Dimensional Applications in Geographical Information Systems. Taylor & Francis, London, pp. 551–577.

Fairfield, J., Leymarie, P., 1991. Drainage networks from grid digital elevation models. Water Resources Research 27, 709–717.

Fette, M., Hoehn, E., Wehrli, B., 2004. Infiltration von flusswasser ins grundwasser. Wasser, Energie, Luft 11/12, 301–304.

Fette, M., Weber, C., Peter, A., Wehrli, B., 2007. Hydropower production and river rehabilitation: a case study on an alpine river. Environmental Modeling and Assessment 12, 257–267.

Florinsky, I.V., Eilers, R.G., Manning, G.R., Fuller, L.G., 2002. Prediction of soil properties by digital terrain modelling. Environmental Modelling & Software 17 (3), 295–311.

Gallant, J.C., Wilson, J.P., 2000. Primary topographic attributes. In: Wilson, J.P., Gallant, J.C. (Eds.), Terrain Analysis. Principles and Applications. John Wiley & Sons, New York, Chichester, pp. 51–86.

Gurtz, J., Baltensweiler, H., Lang, H., Menzel, L., Schulla, J., 1997. Auswirkungen von klimatischen Variationen von Wasserhaushalt und Abfluss im Flussgebiet des Rheins. In: Schlussbericht NFP 31: Klimaänderungen und Naturkatastrophen. vdf Hochschulverlag an der ETH Zürich, Zürich, pp. 1–147.

Haenlein, M., Kaplan, A.M., 2004. A beginner's guide to partial least squares analysis. Understanding Statistics 3, 283–297.

Kenny, F., Matthews, B., Todd, K., 2008. Routing overland flow through sinks and flats in interpolated raster terrain surfaces. Computers & Geosciences 34 (11), 1417–1430.

Klingseisen, B., Metternicht, G., Paulus, G., 2008. Geomorphometric landscape analysis using a semi-automated GIS-approach. Environmental Modelling & Software 23 (1), 109–121.

Kuhn, N.J., Hoffmann, T., Schwanghart, W., Dotterweich, M., 2009. Agricultural soil erosion and global carbon cycle: controversy over? Earth Surface Processes and Landforms 34, 1033–1038.

Lacroix, M.P., Martz, L.W., Kite, G.W., Garbrecht, J., 2002. Using digital terrain analysis modeling techniques for the parameterization of a hydrologic model. Environmental Modelling & Software 17 (2), 125–134.

Loizeau, J.-L., Dominik, J., 2000. Evolution of the Upper Rhone River discharge and suspended sediment load during the last 80 years and some implications for lake Geneva. Aquatic Sciences – Research Across Boundaries 62, 54–67.

Merritt, W.S., Letcher, R.A., Jakeman, A.J., 2003. A review of erosion and sediment transport models. Environmental Modelling & Software 18 (8–9), 761–799. the Modelling of Hydrologic Systems.

Moore, I.D., Grayson, R.B., Ladson, A.R., 1993. Digital terrain modelling: a review of hydrological, geomorphological, and biological applications. In: Beven, K.J., Moore, I.D. (Eds.), Terrain Analysis and Distributed Modelling in Hydrology. Advances in Hydrological Processes. Wiley & Sons, Chichester, New York, Brisbane, pp. 7–34.

Murray, A.B., Lazarus, E., Ashton, A., Baas, A., Coco, G., Coulthard, T., Fonstad, M., Haff, P., McNamara, D., Paola, C., Pelletier, J., Reinhardt, L., 2009. Geomorphology, complexity, and the emerging science of the earth's surface. Geomorphology 103 (3), 496–505.

Nicholas, A.P., 2005. Cellular modelling in fluvial geomorphology. Earth Surface Processes and Landforms 30, 645–649.

Orlandini, S., Moretti, G., Franchini, M., Aldighieri, B., Testa, B., 2003. Path-based methods for the determination of nondispersive drainage direction in grid-based digital elevation models. Water Resources Research 39 (6), 1144.

Pelletier, J., 2008. Quantitative Modeling of Earth Surface Processes. Cambridge University Press, Cambridge.

Pfaundler, M., Zappa, M., 2006. Die mittleren Abflüsse über die ganze Schweiz. Ein optimierter Datensatz im 500 × 500 m Raster. Wasser, Energie, Luft 4, 291–298.

Pullar, D., 2004. Simumap: a computational system for spatial modelling. Environmental Modelling & Software 19 (3), 235–243. Concepts, Methods and Applications in Environmental Model Integration.

Quinn, P., Beven, K., Chevallier, P., Planchon, O., 1993. The prediction of hillslope flow paths for distributed hydrological modelling using digital terrain models. In: Beven, K.J., Moore, I.D. (Eds.), Terrain Analysis and Distributed Modelling in Hydrology. Advances in Hydrological Processes. John Wiley & Sons, Chichester, New York, pp. 63–83.

Rigon, R., Antonello, A., Franceschi, S., 2008. Jgrass: the horton machine. In: Geophysical Research Abstracts, vol. 10, pp. EGU2008–A–09553.

Seibert, J., McGlynn, B.L., 2007. A new triangular multiple flow direction algorithm for computing upslope areas from gridded digital elevation models. Water Resources Research 43, W04501.

Spreaficio, M., Weingartner, R., Leibundgut, C., 1992. Hydrologischer Atlas der Schweiz. EDMZ, Bern. http://www.hades.unibe.ch/hades_d/index.htm.

Strang, G., 2003. Lineare Algebra. Springer, Berlin, Heidelberg, New York.

Tarboton, D.G., 1997. A new method for the determination of flow directions and upslope areas in grid digital elevation models. Water Resources Research 33, 309–319.

Temme, A.J.A.M., Schoorl, J.M., Veldkamp, A., 2006. Algorithm for dealing with depressions in dynamic landscape evolution models. Computers & Geosciences 32, 452–461.

Verbunt, M., Zappa, M., Gurtz, J., Kaufmann, P., 2005. Verification of a coupled hydrometeorological modeling approach for alpine tributaries in the Rhine basin. Journal of Hydrology 324, 224–238.

Vincent, L., 1993. Morphological grayscale reconstruction in image analysis: applications and efficient algorithms. IEEE Transactions on Image Processing 2, 176–201.

Viviroli, D., Zappa, M., Gurtz, J., Weingartner, R., 2009. An introduction to the hydrological modelling system PREVAH and its pre- and post-processing-tools. Environmental Modelling & Software 24 (10), 1209–1222.

Warren, S.D., Hohmann, M.G., Auerswald, K., Mitasova, H., December 2004. An evaluation of methods to determine slope using digital elevation data. CATENA 58 (3), 215–233.

Wold, H., 1975. Path models with latent variables: the NIPALS approach. In: Blalock, H.M., Aganbegian, A., Borodkin, F.M., Boudon, R., Capecchi, V. (Eds.), Quantitative Sociology: International Perspectives on Mathematical and Statistical Modeling. Academic Press, New York, pp. 307–357.

Wu, S., Li, J., Huang, G., 2007. Modeling the effects of elevation data resolution on the performance of topography-based watershed runoff simulation. Environmental Modelling & Software 22 (9), 1250–1260.

Zappa, M., 2002. Multiple-response Verification of a Distributed Hydrological Model at Different Spatial Scales. Ph.D. thesis. ETH Zürich. http://e-collection.ethbib.ethz.ch/view/eth:26410.

Zappa, M., Pos, F., Strasser, U., Warmerdam, P., Gurtz, J., 2003. Seasonal water balance of an alpine catchment as evaluated by different methods for spatially distributed snowmelt modelling. Nordic Hydrology 34, 179–202.